

**Laser-induced fluorescence-line-narrowing studies of impurity-ion systems:  $\text{LaF}_3:\text{Pr}^{3+}$  †**

R. Flach, D. S. Hamilton, P. M. Selzer, and W. M. Yen

*Department of Physics, The University of Wisconsin, Madison, Wisconsin 53706*

(Received 7 July 1976)

The technique of time-resolved fluorescence line narrowing has been applied to the  $^3P_0$  state in  $\text{LaF}_3:\text{Pr}^{3+}$ . Investigations included not only the low-concentration limit, but also samples of higher concentration. By sampling the fluorescence signal very shortly after the excitation pulse, measurements of homogeneous widths were undertaken. It is shown that the effect of "accidental coincidence" plays an important role in the analysis of nonresonant linewidths at low temperatures. Also considered are differences in the dependence of the excited-state energies on the crystal-field strength. By properly accounting for these effects, it is shown that all of our linewidth data can still be explained by the existing theory of phonon-induced relaxation. An extensive discussion is given of time-resolved studies exhibiting the effect of phonon-assisted spectral diffusion. Included are results that have been reported previously. Finally, at higher concentrations, a variety of new effects have been observed. These include "pseudodiffusion," line-shape and linewidth variations in the nonresonant transition, and a variation of the  $1/e$  lifetime of the excited state as a function of the absorption frequency. These effects are attributed to strongly concentration-dependent satellite lines that, at these higher concentrations, are now folded into the broadened main line. It is pointed out that when dealing with conventional line-shape and decay-curve measurements in samples of higher concentration, the possible presence of all of these effects has to be considered and properly accounted for.

**I. INTRODUCTION**

The recent advances in the construction of dye lasers have led to the successful application of new spectroscopic techniques such as saturation spectroscopy,<sup>1</sup> two-photon absorption,<sup>2</sup> and fluorescence line narrowing<sup>3</sup> to overcome the inhomogeneous broadening in gases.

With respect to the application of these same techniques to solid-state spectroscopy, one has to take into account major qualitative and quantitative differences in the spectroscopic behavior. The most important of these is the different nature of the inhomogeneous broadening. Whereas the inhomogeneous broadening is due to the Doppler effect in gases, it is due to strain and other lattice imperfections in solids. Because of this, it is immediately clear that two-photon absorption will not produce line-narrowing phenomena in solids. Considering saturation spectroscopy on the other hand, this method should be able to measure homogeneous widths of absorption lines, if it is modified appropriately.<sup>4</sup> However, there are problems with reaching high enough power levels for the saturation beam, when operating in a pulsed mode.<sup>5</sup> Also this method would not allow the detection of possible hidden hyperfine structures (such as nuclear hyperfine splitting, etc.), which are otherwise masked by the inhomogeneous broadening. The technique of fluorescence line narrowing (FLN) on the other hand does not have any of the disadvantages mentioned above. By sampling the fluorescence profile at different delays after the excitation pulse, it also allows a simple direct

time-resolved study of the fluorescence profile. Moreover it allows the observation of transitions that do not involve the ground state, contrary to the technique of saturation spectroscopy.

Having determined that for the great majority of applications time-resolved FLN is the most versatile of the techniques mentioned above,<sup>6</sup> this method was applied to the case of the  $^3P_0$  state in  $\text{LaF}_3:\text{Pr}^{3+}$ . These investigations included not only the low-concentration limit, but also samples of higher concentration. By sampling the fluorescence signal very shortly after the excitation pulse, studies in homogeneous widths were undertaken. It is shown that the effect of "accidental coincidence" plays an important role in the analysis of nonresonant linewidths at low temperatures. Also considered are differences in the dependence of the excited-state energies on the crystal-field strength. By properly accounting for these effects, it is shown that all of our results can still be explained by the existing theory of phonon-induced relaxation. In addition, a more extensive discussion is given of the effect of phonon-assisted spectral diffusion. This includes results of time-resolved studies reported previously.<sup>7-9</sup> Finally, at higher concentrations, effects such as a variation of the  $1/e$  lifetime across the absorption profile, pseudodiffusion, and variations in linewidth and line shape were observed. These are all processes which have previously not been observable directly with broad-band excitation methods. We also conclude that, when dealing with conventional line shape and decay-curve measurements in samples of higher concentrations, the possible pres-

ence of the type of effects observed in this experiment must be considered and properly accounted for.

## II. EXPERIMENTAL SETUP AND PROCEDURES

Contrary to gases where the largest Doppler widths are on the order of a couple of GHz (e.g.,  $\approx 6$  GHz for hydrogen at room temperature in the visible), inhomogeneous widths of up to  $10 \text{ cm}^{-1}$  are easily possible in solid-state spectroscopy when dealing with higher concentration samples. Because of this, and in order to have a laser that can be scanned repetitively and reliably to any point within the whole inhomogeneous absorption profile, it was necessary to develop a new tuning technique. This was done by the introduction of pressure scanning, and has been described in an earlier publication.<sup>10</sup> For all applications reported here, such a laser, operating in its intermediate resolution mode (roughly 1 to 1.5 GHz) was used.

The experimental setup is shown in Fig. 1. The laser is polarized vertically and focused down on the sample by lens  $F_1$ . The sample itself, with the  $c$  axis horizontal, is mounted on the tip of a variable-temperature cryostat. The fluorescence of the sample is then focused on the entrance aperture  $A_1$  of a Fabry-Perot interferometer via lenses  $F_3$  and  $F_4$ . The diameter of aperture  $A_1$  is chosen to give a resolution of at least  $0.7 R_0$ , where  $R_0$  is the maximum, reflectivity-limited resolution of the Fabry-Perot. The Fabry-Perot interferometer itself is pressure scanned and has an effective open-plate diameter of 5 cm. Its nominal surface flatness is  $\lambda/100$ , or better. With plate reflectivities of (91.5 or 93.5)%, the etalon spacing was varied between 0.2 and 30 mm, depending on the desired resolution, free spectral range, and signal-to-noise ratio. After having passed through the collimating lens  $F_5$  and the etalon assembly, the fluorescence light is re-focused onto the aperture  $A_2$ , which eliminates undesired back reflections emanating primarily from the back surfaces of the Fabry-Perot plates. Before reaching the photomultiplier, the fluorescence light is collimated once more (collimating lens  $F_7$ ) to fall through an appropriate 1-in.-diam interference filter (full bandwidth at half-maximum: 6 to  $10 \text{ \AA}$ ). This interference filter eliminates all the fluorescence light except for the one particular fluorescence line under investigation. After having been detected with the photomultiplier, the fluorescence signal is passed through a current-to-voltage converter and amplified (amplifier: Keithley, Model 104). To prevent saturation of the electronics because of scattered

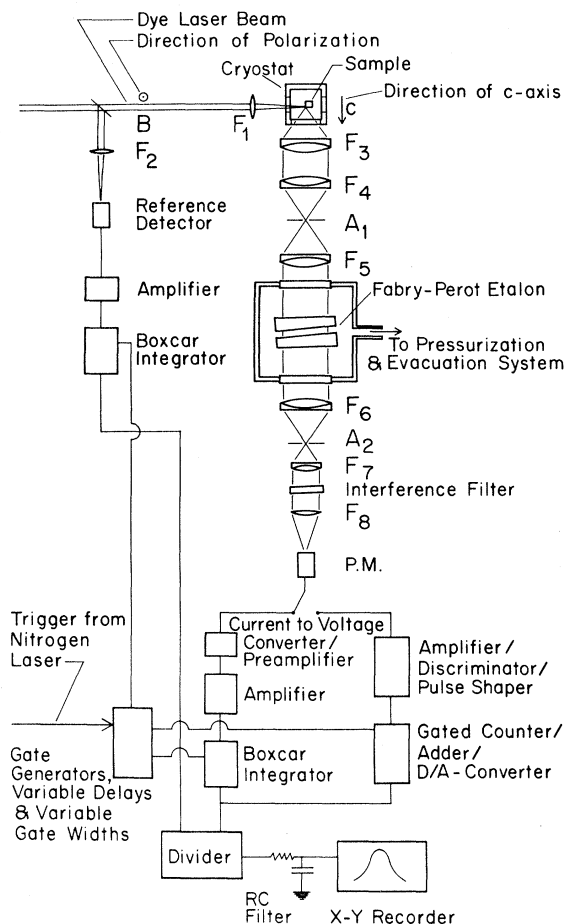


FIG. 1. Experimental setup.  $F_1$ – $F_8$ : Focusing and collimating lenses.  $B$ : Beamsplitter.  $A_1$  and  $A_2$ : Apertures. The dye laser is described in Ref. 10.

laser light that reaches the photomultiplier when doing measurements on the resonant transition, a system of diodes and appropriate resistors is used in the current-to-voltage converter and the pre-amplifier. This system reduced the saturation of the current-to-voltage converter and the pre-amplifier to less than  $1.5 \mu \text{ sec}$  even under the most severe conditions. Finally, the signal is fed into a box-car integrator (Moletron, Model 112 Differential Gated Integrator) where it is sampled at a preset time delay  $t$  after the excitation pulse.

By repeatedly scanning the interferometer at different time delays, the  $t=0$  characteristics as well as the whole time evolution of the fluorescence profile can then be recorded. Because of considerable fluctuations in dye laser power, the signal-to-noise ratio is improved by dividing the output of the box-car integrator with a reference. (For most applications this division was done digitally using a combination of two analog-to-frequency converters, a Hewlett-Packard 5326 A timer-counter, and a digital-

to-analog converter.) The output of the divider is then passed through an RC filter, and finally displayed on an X-Y recorder.

Because of low signal levels, some of the data for the low-concentration samples was also taken using photon counting. For this purpose an exactly complementary system to the one described above was used, consisting of an amplifier-discriminator-pulshaper combination (SSR-1120 Amplifier-Discriminator), a gated counter-adder, and a digital-to-analog converter. This system is also indicated in Fig. 1.

The system studied,  $\text{LaF}_3:\text{Pr}^{3+}$ , was chosen for the following reasons: (a)  $\text{Pr}^{3+}$  is one of the most soluble rare-earth ions in  $\text{LaF}_3$ , and no clustering is observed at any concentration. This allows a direct concentration-dependent study of ion-ion interactions, giving new insight into such processes as energy migration and spectral diffusion.<sup>7</sup> (b) The properties of the most important fluorescence lines, in particular their shape, shift, and widths, are relatively well known, and have been investigated.<sup>11</sup> (c) Also, the state initially excited in our experiment, the  $^3P_0$  level (see Fig. 2), is in a wavelength region where pulsed dye lasers can be operated without any difficulties.

The approximate position of the Stark manifolds of  $\text{Pr}^{3+}$  (host:  $\text{LaF}_3$ ) are shown in Fig. 2. Being a non-Kramers ion, the low crystalline-field symmetry ( $C_2$ ) in  $\text{LaF}_3$  lifts all degeneracies. Each Stark manifold is therefore split into  $2J+1$  individual components, where  $J$  is the total angular momentum quantum number. With the laser pumping into the  $^3P_0$  state (lifetime:  $\tau_0 \approx 50 \mu\text{sec}$ ) at  $4777.7 \text{ \AA}$ , two inhomogeneously broadened lines were investigated: The nonresonant transition to the lowest level ( $^3H_6$ )<sub>1</sub> of the  $^3H_6$  manifold, at  $5985.3 \text{ \AA}$ , and the resonant transition back to the ground state ( $^3H_4$ )<sub>1</sub>. A  $\frac{1}{4}$ - $\mu\text{sec}$  gate aperture was used for most measurements. The laser-dye solution consisted of roughly  $5 \times 10^{-3}$  mol/l coumarin 1F (7-diethylamino-4-trifluoromethylcoumarin) in *p*-Dioxane, giving a peak output power of approximately 1.5 to 2 kW. The possible presence and distorting influence of nonlinear phenomena such as lasing (e.g., in the  $^3P_0 \rightarrow ^3H_6$  transitions),<sup>12</sup> photon echoes,<sup>13</sup> and self-induced transparency<sup>14</sup> were checked, and found to be negligible. The dopant concentration of most samples (single crystals obtained from Optovac, Inc.) was 0.2 and 5 mol%, with some more recent studies done at a concentration of 20 mol%.<sup>9</sup>

### III. STUDIES OF HOMOGENEOUS WIDTHS

In this section we discuss the experimental results of line shapes and homogeneous widths.

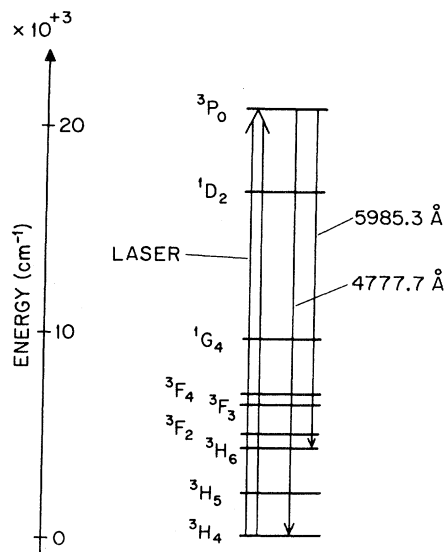


FIG. 2. Approximate position of the Stark manifolds of  $\text{Pr}^{3+}$  in  $\text{LaF}_3$ . With the laser pumping into the  $^3P_0$  state at approx.  $4777.7 \text{ \AA}$ , two inhomogeneously broadened transitions are investigated: The nonresonant transition to the lowest level ( $^3H_6$ )<sub>1</sub> of the  $^3H_6$  manifold, at approx.  $5985.3 \text{ \AA}$ , and the resonant transition back to the ground state ( $^3H_4$ )<sub>1</sub>.

As mentioned previously, these studies were done by sampling the fluorescence signal very shortly (500 nsec–2  $\mu\text{sec}$ ) following the laser excitation pulse. The two transitions investigated showed various degrees of line narrowing dependent on temperature and concentration.

#### A. Residual widths at low temperature

At low temperatures the resonant transition  $^3P_0 \rightarrow (^3H_4)_1$  exhibits strong line narrowing. We obtain an upper limit of 200 MHz for its width at 4.8 K and a concentration of 5 mol%. At the same temperature the nonresonant transition  $^3P_0 \rightarrow (^3H_6)_1$ , on the other hand, shows some unexpectedly large residual widths; we get a width of  $\approx 1.3 \text{ GHz}$  for the 0.2-mol% sample, and a much larger width of  $\approx 1 \text{ cm}^{-1}$  for the 5-mol% sample. These widths as well as corresponding line shape and linewidth variations observed for the 5-mol% sample are illustrated in Figs. 3 (Ref. 15) and Fig. 4.

To understand these unexpectedly large residual widths in the nonresonant transition (as well as the corresponding line shape and linewidth variations depicted in Fig. 4), we first address ourselves to the case of the 0.2-mol% sample. Although it is clear that the theory of phonon-induced relaxation<sup>11</sup> is not able to account for this large residual width, it may still be argued that it results from

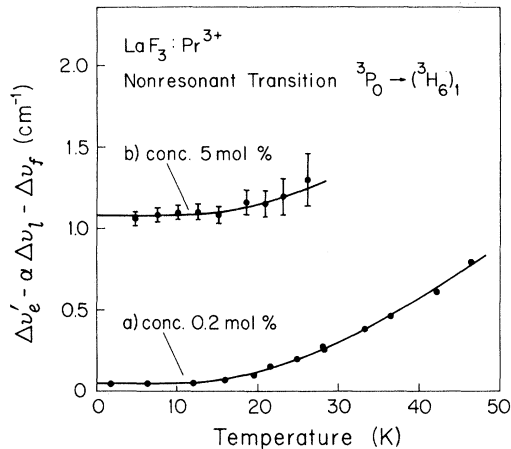


FIG. 3. Temperature dependence of the width of the nonresonant transition  ${}^3P_0 \rightarrow ({}^3H_6)_1$ . The symbols  $\Delta\nu'_e$ ,  $\Delta\nu'_l$ ,  $\Delta\nu'_f$  and  $\alpha$  are explained in the text [see Eqs. (1) and (2)]. The widths were measured for two different samples: (a) concentration 0.2 mol%, and (b) concentration 5 mol%. The solid curves indicate the result of Eq. (4). For position of the laser frequency relative to the center of the  $({}^3H_4)_1 \rightarrow {}^3P_0$  absorption profile see Ref. 15.

a very high multiphonon decay rate from the  $({}^3H_6)_1$  level to the next lower Stark manifold. However, the lifetime of the  $({}^3H_6)_1$  level has been measured<sup>16</sup> for  $\text{LaCl}_3:\text{Pr}^{3+}$ , giving a value on the order of  $10^{-2}$  sec. Taking into account the differences in multiphonon relaxation rate between the  $\text{LaF}_3$  and  $\text{LaCl}_3$  lattices,<sup>17</sup> we get an estimated lifetime of  $20 \times 10^{-6}$  sec. This is five orders of magnitude slower than the value of  $0.12 \times 10^{-9}$  sec necessary to account for the observed linewidth. In addition, if the residual width is attributed to a fast lifetime-limiting decay rate, the corresponding line shape would have to be Lorentzian. However, our measurements show that the line shape is non-Lorentzian, clearly indicating that the mechanism has to be of a different nature than the one discussed above. It might also be postulated that the large residual width is due to unresolved nuclear hyperfine splitting, the latter being unexpectedly large in case of the  ${}^3P_0 \rightarrow ({}^3H_6)_1$  nonresonant transition. However, recent measurements of Erickson<sup>18</sup> have shown that this splitting is negligibly small.<sup>19</sup> Throughout this paper, nuclear hyperfine splitting (and related effects) will thus be neglected.

Next we address ourselves to the case of the 5-mol% sample, where we have observed an even larger residual width of roughly  $1 \text{ cm}^{-1}$ . Here, we might possibly assume that the residual width is due to some concentration-dependent broadening mechanism, i.e., either resonance broadening or cross relaxation. Since cross relaxation of

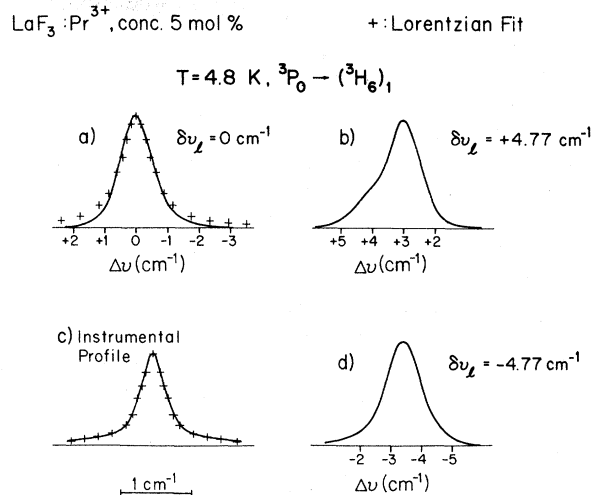


FIG. 4. Linewidth and line shape variations in the nonresonant transition  ${}^3P_0 \rightarrow ({}^3H_6)_1$ . The symbol + indicates a Lorentzian fit.  $\delta\nu_L$  is the shift of the laser frequency relative to the center of the  $({}^3H_4)_1 \rightarrow {}^3P_0$  absorption profile. The linewidth varies from  $\Delta\nu_a \approx 0.8 \text{ cm}^{-1}$  at (a) to  $\Delta\nu_a \approx 1.1 \text{ cm}^{-1}$  at (d) [ $\Delta\nu_a$  is the residual width due to accidental coincidence, see Eq. (2)]. The asymmetry in (b) is clearly connected to the effect of "pseudodiffusion" which is discussed in Sec. V.

this magnitude would almost totally quench the  ${}^3P_0$  state, it must be argued that this cross relaxation would originate from the terminal  $({}^3H_6)_1$  level. However, the most favorable relaxation scheme for this level, namely,  $({}^3H_6)_1 + ({}^3H_4)_1 \rightarrow ({}^3H_5)_1 + ({}^3H_5)_1$ , has an energy deficit (i.e., activation energy) of  $135 \text{ cm}^{-1}$ , making it a highly unlikely process in the temperature range of interest. Resonance broadening on the other hand would indicate a strong coupling between  $\text{Pr}^{3+}$  ions giving rise to excitonlike behavior and hence, dispersion in the excited states. However, a dispersion of  $1 \text{ cm}^{-1}$  corresponds to an interaction strength of roughly  $1 \text{ cm}^{-1}$ , which is considerably stronger than the interaction strength between nearest-neighbor rare-earth ions (typically estimated at  $10^{-1}$  to  $10^{-2} \text{ cm}^{-1}$ ). Therefore in these dilute inhomogeneously broadened systems, the dispersion would be expected to be even smaller. We thus conclude that resonance broadening is not the cause of our observations. This will be further substantiated by the fact that we can account below for all of our observations by the theory of phonon-induced relaxation with the exception of the large residual widths that are discussed in this paragraph.

To understand our results, we follow the treatment of Motegi and Shionoya,<sup>20</sup> who have shown that using FLN techniques it is possible to map the energy-level schemes of inhomogeneously

broadened systems. Such a mapping is illustrated in Fig. 5. In essence, Fig. 5 shows the shift of the center of the  ${}^3P_0 \rightarrow ({}^3H_6)_1$  fluorescence line relative to the corresponding shifts in the  $({}^3H_4)_1 \rightarrow {}^3P_0$  excitation frequency. The abscissa, i.e., the "crystal-field-strength" parameter, is a virtual parameter indicating the "strength" of the crystal field. Had our system been a gas, this parameter would have been the axial velocity. The solid analog to a gas would then be a system where the entire crystalline-field environment is determined by *one* parameter only. Moreover in such a system all the inhomogeneous broadening could only arise from variations of this parameter characterizing the crystalline-field environment, i.e., it could not also be due to slight distortions resulting in various small deviations from the nominal site symmetry. It is clear that for all practical purposes no actual system is able to fulfill these requirements. In particular the system under investigation,  $\text{LaF}_3:\text{Pr}^{3+}$  (most probable site symmetry:  $C_2$ )<sup>21</sup> has more than 10 free crystalline-field parameters. This fact is of singular importance, since it devaluates *a priori* the exactness of the type of representation shown in Fig. 5. In contrast to the case of a true one-parameter system such as a gas, this makes it possible for two ions to absorb in resonance, even though they may be in sites having two different sets of crystalline-field parameters. These two ions will then generally emit to slightly different

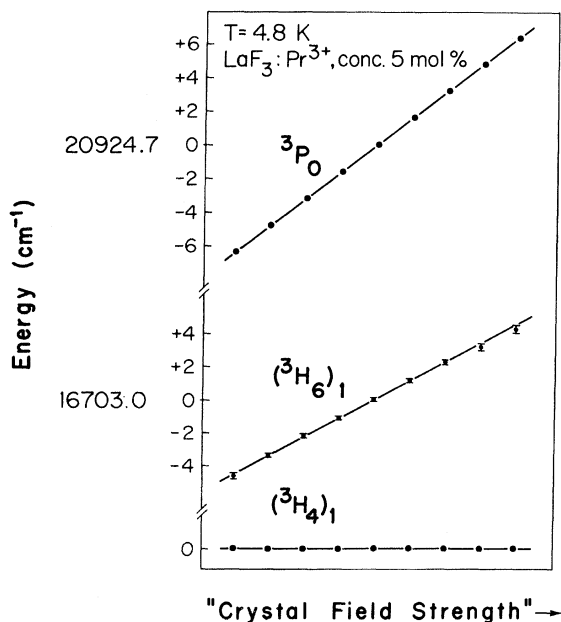


FIG. 5. Mapping of the  $\text{Pr}^{3+}$  energy-level scheme following the treatment of Ref. 20. The concentration is 5 mol% and the temperature 4.8 K.

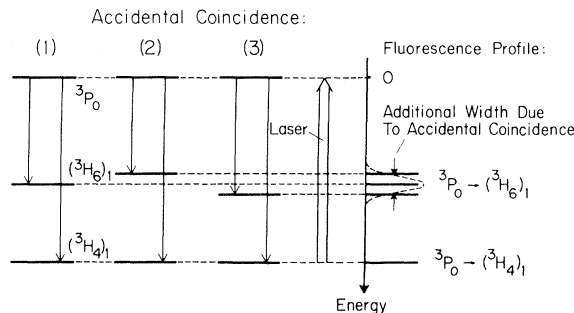


FIG. 6. Graphic illustration of the effect termed "accidental coincidence" (see text). Although ions (1), (2), and (3) all absorb in resonance, they emit to slightly different nonresonant levels. This gives rise to the residual width indicated on the right-hand side of the figure.

nonresonant levels, thus giving rise to the residual widths observed here in our experiment. This situation, termed "accidental coincidence," is indicated in Fig. 6.<sup>22</sup>

This interpretation is consistent with all our other observations noted previously. In particular, due to the static nature of the effect, we would expect the resultant line shapes to be non-Lorentzian. That this is indeed the case can be seen from Fig. 4. We would also expect that the amount of "accidental coincidence" is to be correlated in some sense to the gross inhomogeneous width of the absorption line. (The inhomogeneous width of the absorption line may be looked upon as a "measure" of the overall site to site variations in the crystalline-field parameters.) Accordingly we observed a strong increase in the inhomogeneous width of the  $({}^3H_4)_1 \rightarrow {}^3P_0$  absorption line when the concentration was increased to 5 mol%. We attribute then the strong increase of the residual width with concentration (Fig. 3) to this increase in the inhomogeneous width of the absorption line.

We conclude, in dealing with FLN experiments in solids, that care must be exercised in the analysis of all nonresonant transitions. This is in contrast to the resonant transition, which, in general, still reflects the true homogeneous width of the absorption line.

#### B. Temperature-dependent linewidth data

Having determined the nature of the residual widths, we now proceed to investigate the correct fitting procedure for our linewidth data. This is done using the theory of phonon-induced relaxation.<sup>11</sup> These processes lead to purely homogeneous broadening of the transitions and are known to have well-defined temperature dependences. For all of our treatments here, we have assumed that the line shapes involved are Lorentzian (to

the extent that, within the experimental accuracy, the convolution of any two lines has a width equal to the sum of the individual linewidths). This includes the assumption that  $\Delta\nu_i + \Delta\nu \ll \Delta\nu_{\text{inh}}$  within the temperature range of interest.  $\Delta\nu_i$  is the laser bandwidth,  $\Delta\nu$  is the homogeneous width of the resonance transition, and  $\Delta\nu_{\text{inh}}$  is the inhomogeneous width of the resonance transition.

Referring again to Fig. 5, it is clear that for the resonance transition we still have<sup>23</sup>

$$\Delta\nu_e = 2\Delta\nu + \Delta\nu_i. \quad (1)$$

Here  $\Delta\nu_e$  is the experimental, i.e., measured width of the transition.  $\Delta\nu_i$  is the sum of  $\Delta\nu_i$  and the instrumental width of the analyzing Fabry-Perot interferometer  $\Delta\nu_f$ .

For the nonresonant transition however, we must account now for differences in slope between the  $(^3H_6)_1$  and  $^3P_0$  levels (Fig. 5); this results in

$$\Delta\nu'_e = \alpha(\Delta\nu + \Delta\nu_i) + \Delta\nu' + \Delta\nu_f + \Delta\nu_a. \quad (2)$$

$$\Delta\nu'_e - \alpha\Delta\nu_i - \Delta\nu_f = \alpha\Delta\nu + \Delta\nu' + \Delta\nu_a$$

$$= 0.703 \times 3.5p_0(66, T) + 1.05p_0(44, T) + \left\{ \begin{array}{l} 0.0435, \text{ concentration } 0.2 \text{ mol\%} \\ 1.08, \text{ concentration } 5 \text{ mol\%} \end{array} \right\} \text{ cm}^{-1}, \quad (4)$$

i.e.,

$$\Delta\nu' = 1.05p_0(44, T) \text{ cm}^{-1}. \quad (5)$$

$p_0(w_i, T)$  is given by

$$p_0(w_i, T) = [\exp(w_i/kT) - 1]^{-1}, \quad (6)$$

where  $w_i$  is the energy separation between the  $i$ th level and the lowest level within a given Stark manifold,  $k$  is the Boltzmann constant, and  $T$  is the temperature. Equations (3) and (4) are indicated as the solid curves in Figs. 7 and 3, respectively. Equation (3) was obtained by considering the center of gravity of the second and third levels (resulting in  $w'_2 \cong 66 \text{ cm}^{-1}$ ) and by neglecting the contribution of all higher levels. The fourth level, in particular, is  $137 \text{ cm}^{-1}$  above the ground state, and by using the numbers of Ref. 11 it can be shown that its contribution amounts to less than 1% at 45 K. To obtain the results of Eq. (4), the value of  $\alpha$ —the ratio of the slopes between the  $(^3H_6)_1$  and the  $^3P_0$  levels—had to be determined more accurately. This is shown in Fig. 8. As can be seen from this figure, all the points lie on a straight line, with the exception of those farthest from the center frequency of the absorption line. The value of  $\alpha$  extracted from Fig. 8 is  $\alpha = 0.703 \pm 0.012$ . This is less than what we would have expected, had our system been a gas; in such a case the value of  $\alpha$ , to first order,

Here  $\Delta\nu'_e$  is the measured width of the nonresonant transition, and  $\alpha$  is the ratio of the slopes between the  $(^3H_6)_1$  and the  $^3P_0$  levels.  $\Delta\nu'$  is the homogeneous width of the nonresonant transition. The term  $\Delta\nu_a$  is the additional width due to accidental coincidence discussed in the previous paragraph. To within a good approximation,  $\Delta\nu_a$  will be a temperature-independent factor.<sup>24</sup> We note that, apart from  $\Delta\nu'$  and  $\Delta\nu_a$ , the experimental width  $\Delta\nu'_e$  is also dependent on  $\Delta\nu$  and  $\alpha$ . The latter two parameters must therefore be known first, before an accurate determination of  $\Delta\nu'$  can be made through Eq. (2).

If we now follow the treatment of Ref. 11, it can be shown that all Raman terms can be neglected within the temperature range of interest,<sup>25</sup> which leaves only the contribution of the direct process. From the data of Figs. 7 and 3 we obtain then for the resonant transition  $^3P_0 \rightarrow (^3H_4)_1$ ,

$$\frac{1}{2}(\Delta\nu_e - \Delta\nu_i) = \Delta\nu = 3.5p_0(66, T) \text{ cm}^{-1}, \quad (3)$$

and for the nonresonant transition  $^3P_0 \rightarrow (^3H_6)_1$ ,

would have been  $\alpha = \sigma_n/\sigma_r = 0.798$ .  $\sigma_r$  and  $\sigma_n$  are the energies of the resonant and nonresonant transitions, respectively. It was found that an adequate fit could be obtained for Eq. (4) [and Eq. (5) as well] by only considering the second Stark level of the  $^3H_6$  manifold. This was done, although Ref. 11 indicates that the contribution of

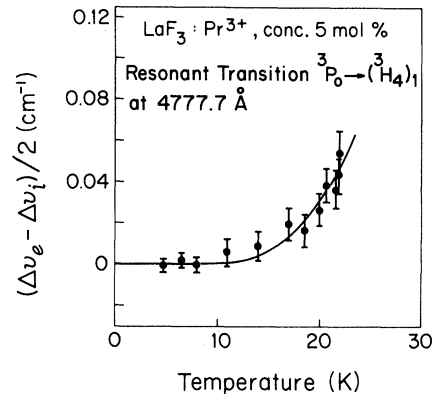


FIG. 7. Temperature dependence of the width of the resonant transition  $^3P_0 \rightarrow (^3H_4)_1$ .  $\Delta\nu_e$  is the experimental, i.e., measured width, and  $\Delta\nu_i$  is the instrumental width (see text). The solid curve indicates the result of Eq. (3). The concentration is 5 mol %. The data are taken with the laser pumping in the center of the  $(^3H_4)_1 \rightarrow ^3P_0$  absorption line.

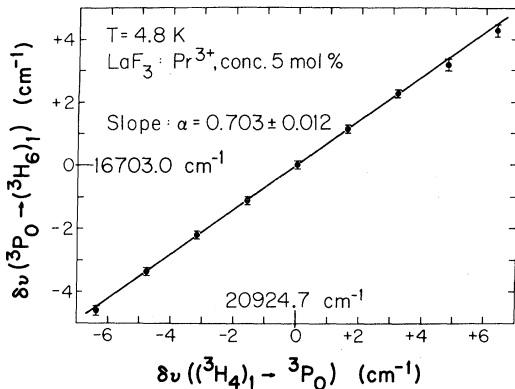


FIG. 8. Shift of the center of the  ${}^3P_0 \rightarrow ({}^3H_6)_1$  nonresonant fluorescence profile plotted vs the  $({}^3H_4)_1 \rightarrow {}^3P_0$  laser-excitation frequency. The resultant slope is equal to  $\alpha$ —the ratio of the slopes between the  $({}^3H_6)_1$  and  ${}^3P_0$  levels in Fig. 5—giving  $\alpha = 0.703 \pm 0.012$ . The concentration is 5 mol% and the temperature 4.8 K.

the third level is no longer negligible in the temperature range of interest. Quite generally we note, by comparing the direct process coefficients of Eqs. (3) and (5) with those of Yen *et al.*,<sup>11</sup> that the latter are consistently higher. We attribute this to the fact that the coefficients of Ref. 11 were deduced by assuming a constant inhomogeneous width  $\Delta\nu_{inh}$ , although  $\Delta\nu_{inh}$  varies with wavelength, the specific transition involved, and the concentration. It might also have been necessary in Ref. 11 to include not only the direct process coefficients to the two or three lowest levels, but also the ones connecting to the remaining higher levels within the same Stark manifold. This is true for any accurate investigation extending to higher temperatures.

From Figs. 3 and 7 we note that our data provides good agreement with theory (solid lines). We conclude therefore that, by properly accounting for the peculiarities that occur when the technique of fluorescence line narrowing is applied to solids, all of our results can still be explained by the existing theory of phonon-induced relaxation.

Not discussed so far are the linewidth and line-shape variations observed when the laser is pumping at different positions in the  $({}^3H_4)_1 \rightarrow {}^3P_0$  absorption line. These changes are indicated in Fig. 4. The variations in linewidth are due to corresponding changes in  $\Delta\nu_a$  [see Eqs. (2) and (4)]. These changes in  $\Delta\nu_a$  may (at least in part) be explained by the presence of very strong satellite lines that, at these higher concentrations, are now folded into the strongly broadened main line. The presence of these satellite lines is discussed in Sec. V. The variations in line shape can be attributed to the presence of these satellite

lines as well. This is evident for the case of the fluorescence profile at  $\delta\nu_l = +4.77 \text{ cm}^{-1}$  [see Fig. 4;  $\delta\nu_l$  is the frequency of the laser with respect to the center of the  $({}^3H_4)_1 \rightarrow {}^3P_0$  absorption profile] where the corresponding asymmetry is clearly connected to the effect of “pseudodiffusion” discussed in Sec. V.

#### IV. TIME-RESOLVED STUDIES

In this section we give a short review of the time-resolved studies that have been published previously,<sup>7,9</sup> together with additional remarks that had not been included because of the limited space available.

Figure 9 shows typical results of time-resolved studies taken with a Fabry-Perot interferometer on the resonant transition  ${}^3P_0 \rightarrow ({}^3H_4)_1$ . The temperature is 17 and 35 K, respectively, and the concentration of the sample is 5 mol%. Figure 10 shows similar results taken with a 1-m grating spectrometer on the nonresonant transition  ${}^3P_0 \rightarrow ({}^3H_6)_1$ . The concentration of the sample is 20 mol%, and the laser is pumping at two different positions ( $\pm 6 \text{ cm}^{-1}$  off center) within the inhomogeneously broadened absorption line. To analyze our results, we have assumed that the strain broadening is microscopic, i.e., that it is random over a characteristic distance smaller than the average ion-ion separation. Assuming that the

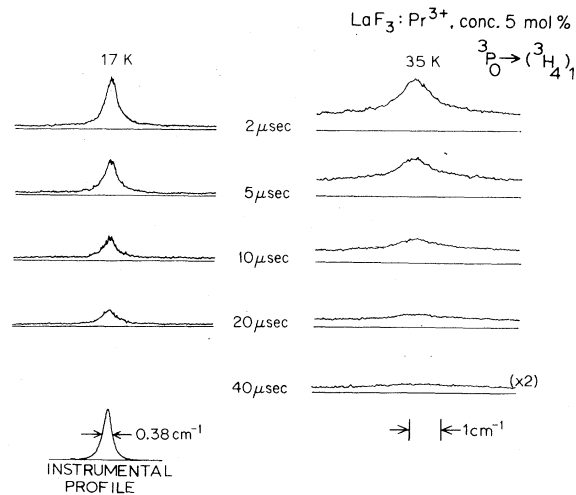


FIG. 9. Typical results of time-resolved studies taken with a Fabry-Perot interferometer on the resonant transition  ${}^3P_0 \rightarrow ({}^3H_4)_1$ . The concentration of the sample is 5 mol%. The laser is pumping in the center of the  $({}^3H_4)_1 \rightarrow {}^3P_0$  absorption profile. The virtually flat shape of the background is due to overlapping orders in the interferometer. The width of the narrowed fluorescence at a given temperature is equal to twice the homogeneous width plus the instrumental profile (see Sec. III). The temperature is 17 and 35 K, respectively.

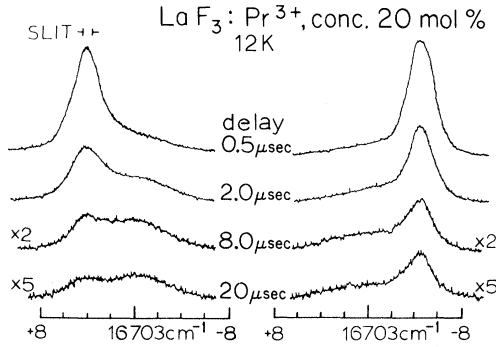


FIG. 10. Results of time-resolved studies taken with a spectrometer on the nonresonant transition  ${}^3P_0 \rightarrow ({}^3H_6)_1$ . The concentration of the sample is 20 mol%. The laser is operating  $6 \text{ cm}^{-1}$  above (left) and below (right) the center of the  $({}^3H_4)_1 \rightarrow {}^3P_0$  absorption profile. A large difference in the transfer rates between these two positions can be detected. The temperature is 12 K.

ion-ion interaction is electrostatic (exchange interaction is thought to be negligible for dilute rare-earth systems as in our case) the transfer rate  $P_{1-2}$  between two ions 1 and 2 can be written as<sup>26,27</sup>

$$P_{1-2} = K(\Delta E, T)R^{-s}. \quad (7)$$

$K(\Delta E, T)$  is a function of the energy mismatch  $\Delta E = E_1 - E_2$ , where  $E_1$  and  $E_2$  are the excitation energies of the two ions. Its qualitative behavior is determined by the transfer mechanism that gives rise to our observations.  $R$  is the inter-ion spacing and  $s$  is equal to 6, 8, or 10 depending on the multipolar nature of the interaction. From the appearance of the full inhomogeneous background at the earliest delays in all of our data we conclude that  $K(\Delta E, T)$  is virtually independent of  $\Delta E$ . This is in contrast to the case of resonance energy transfer by spectral overlap, where  $K(\Delta E, T)$  is a Lorentzian with a width twice the homogeneous width,  $\Delta\nu$ , of the  $({}^3H_4)_1 \rightarrow {}^3P_0$  absorption line.<sup>20,26</sup> In the latter case, instead of a background of the full inhomogeneous width we would have expected a gradual increase in the actual width of the fluorescence line with increasing time delay. However, no such increase is observed at any temperature. This is true in particular for  $T = 40 \text{ K}$ , where the homogeneous width  $\Delta\nu$  is on the order of the instrument profile of the Fabry-Perot interferometer (Fig. 9) and where any presence of resonance transfer would be particularly easy to detect. This absence of resonance energy transfer is in accordance with our calculations, which give an upper limit of  $2 \times 10^{-2} \text{ cm}^{-1}/\mu\text{sec}$  for this increase in linewidth.<sup>7,26</sup>

To get further insight into the transfer mechanism responsible for our observations, its tem-

perature dependence was determined. This was done by treating the initially excited ions, i.e., the ions which give rise to the line-narrowed part of the fluorescence, as the "donor" system. All the other ions were treated as the "acceptor" system. "Donor-donor" transfer is negligible due to the absence of resonance energy transfer. The formula of Inokuti and Hirayama<sup>28</sup> could therefore be applied to the height of the narrowed fluorescence. Following this formula, a least-squares fit was made to a plot of  $-\ln[H(t) + t/\tau_0]$  vs  $t^{3/s}$ , where  $H(t)$  is the height of the narrowed fluorescence, and  $\tau_0$  is the lifetime. If  $\beta$  is the slope of this curve, we then have  $|\beta|^{s/3} = W_T$ , where  $W_T$  is the transfer rate.  $W_T$  is related to  $K(\Delta E, T) = K_0(T)$  via

$$W_T = K_0(T) \left[ \frac{4}{3} \pi C \Gamma(1 - 3/s) \right]^{s/3}. \quad (8)$$

Here  $C$  is the concentration, and  $\Gamma(1 - 3/s)$  is the gamma function. At lower temperatures a dependence of  $K(\Delta E, T)$  on  $\Delta E$  might have been present, although not obvious from our data.<sup>29</sup> In this case it was assumed that  $K_0(T)$  in Eq. (8) can be replaced by a suitable average of  $K(\Delta E, T)$  over  $\Delta E$ .<sup>30</sup> This average may then have a different temperature dependence than  $K(\Delta E, T)$  at fixed  $\Delta E$ , and a comparison between experiment and theory is more difficult. In particular, for the direct process,<sup>27</sup>  $K(\Delta E, T)$  can only be expected to be independent of  $\Delta E$  for  $kT \gg \Delta E$ . This region starts approximately at 30 K for the 5-mol% sample, and at 50 K for the 20-mol% sample. Moreover, deviations from the formula of Inokuti and Hirayama occur at the very earliest delays.<sup>31</sup> These were taken into account by neglecting the corresponding values of  $H(t)$  at these early delays. Finally, not yet considered is the fact that "acceptor-donor" transfer, i.e., back transfer, is not negligible in our case, contrary to the assumption made in the derivation of the above formula. To our knowledge there is no theoretical treatment that takes this fact into account. It was assumed that most of the influence of back transfer was eliminated along with the deviations discussed above, and that any possible residual effect would only manifest itself as a multiplicative factor, therefore not affecting the qualitative behavior of  $W_T$  within the experimental accuracy.

The temperature dependence of the transfer rate  $W_T$  thus obtained is shown in Figs. 11 and 12.<sup>32</sup> Not included in these figures is an apparent additional residual transfer rate which appeared at low temperatures. This transfer rate is due to cross relaxation to the  ${}^1G_4$  level (see Sec. V), and its effect was properly accounted for. The qualitative behavior of  $K_0(T)$  deduced from Figs. 11 and 12 is somewhat different for the 20-mol% sample

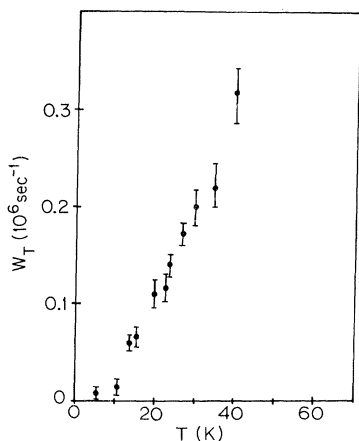


FIG. 11. Temperature dependence of the transfer rate  $W_T$ . The concentration is 5 mol%.

than it is for the 5-mol% sample. This can be attributed to differences in  $\Delta\nu_{\text{inh}}$ , which cause the corresponding averages of  $K(\Delta E, T)$  over  $\Delta E$  to differ, in those cases where  $K(\Delta E, T)$  depends on  $\Delta E$ .

As has been mentioned, resonance energy transfer cannot account for our observations. We therefore consider another possibility, namely phonon-assisted energy transfer. This process can either be direct, or of higher order. The direct process,<sup>27</sup> for  $kT \ll \Delta\nu_{\text{inh}}$ , should lead to a strongly asymmetric background, and a large difference between the transfer rates when the laser is pumping on the high- and low-energy side of the absorption profile. For the 5-mol% sample such an observation is however complicated by the fact that below 7 K, where this asymmetry should appear, the background has already become vanishingly small. Also, for the

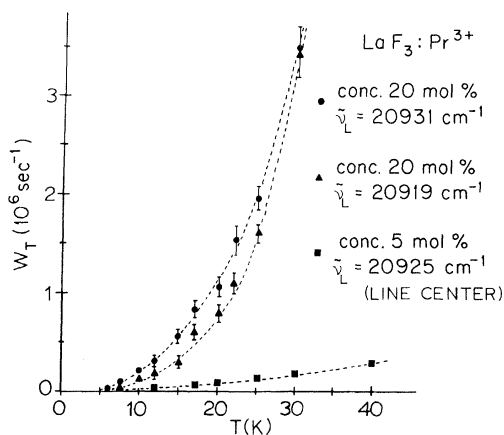


FIG. 12. Temperature dependence of the transfer rate  $W_T$ . The concentration is 20 mol%. The transfer rate of the 5-mol% sample is also indicated for comparison.

5-mol% sample, a search for variations in transfer rate is complicated by the fact that the excited-state lifetime varies with absorption frequency (see Sec. V). For the 20-mol% sample, however, a corresponding variation in transfer rate has been observed,<sup>9</sup> and it is indicated in Fig. 12 (see also Fig. 10). Considering next the temperature dependence of  $W_T$ , the direct process should lead to<sup>20,27</sup>  $W_T \propto T$  for  $kT \gg \Delta\nu_{\text{inh}}$ . This is however not the case, as can be seen from Figs. 11 and 12. Also, for the direct process, the transfer rate asymmetry shown in Fig. 12 would likely persist to  $T=0$  K,<sup>27</sup> which is not observed. An estimate of this residual transfer, from the value at  $T=30$  K, further gives a lower limit of  $W_{T=0} = 0.1 - 0.2 \mu\text{sec}^{-1}$  in Fig. 12. A transfer rate of this magnitude would have been detectable in our experiment, if it had been present. This suggests invoking a second-order phonon process. However, such a process would probably lead to a steeper temperature dependence (either exponential or approaching  $T^7$  for Raman behavior). Taking into account all of these observations, it is felt at the present time that a combination of these phonon-assisted processes will produce the observed behavior.

Other processes not yet considered are virtual phonon exchange and radiation trapping. Virtual phonon exchange is assumed to be negligible in our case.<sup>33</sup> Since the weak resonance fluorescence represents less than 0.1% of the total [the same is also true for the weak  ${}^3P_0 \rightarrow ({}^3H_4)_2$  and  ${}^3P_0 \rightarrow ({}^3H_4)_3$  transitions], the influence of radiation trapping on the time evolution of the fluorescence profile is negligible. To further prevent any distortions in the fluorescence profile of the resonance transition (see, e.g., Fig. 9) all observations were done with  $\Delta\nu_l + 2\Delta\nu \ll \Delta\nu_{\text{inh}}$  (see Sec. III), and with the laser beam exciting the sample very close to its front surface (see Fig. 1). Furthermore, because of the effect of "pseudo-diffusion" (see Sec. V) all observations for the 5-mol% sample were done on the resonant transition and in the center of the  $({}^3H_4)_1 \rightarrow {}^3P_0$  absorption profile. For the 20-mol% sample, however, such effects could be neglected, since it had a much higher transfer rate  $W_T$ . All observations pertaining to the 20-mol% sample were then done on the nonresonant transition  ${}^3P_0 \rightarrow ({}^3H_6)_1$  and with the laser operating 6  $\text{cm}^{-1}$  above and below the center of the  $({}^3H_4)_1 \rightarrow {}^3P_0$  absorption curve (see Fig. 10).

At first glance another possible interpretation of our results might be two-photon absorption into the  $4f5d$  band. However, the  $4f5d$  absorption band ranges from 51 300 to 69 000  $\text{cm}^{-1}$  which is too high by nearly 10 000  $\text{cm}^{-1}$ .<sup>34</sup> Also too high is the  ${}^1S_0$  state, which is located at 46 896  $\text{cm}^{-1}$ .<sup>35</sup>

In conclusion, it would be interesting to extend our type of investigation to other rare-earth and transition-metal ions. It is conceivable that the type of energy transfer process observed in this experiment does exist in other systems and under other conditions as well, and that it might actually dominate the diffusion process in cases where hitherto resonance energy transfer was thought to be the prevalent mechanism.

#### V. STUDIES IN LIFETIMES, PSEUDODIFFUSION, AND RELATED EFFECTS

In this section we discuss effects such as variations in the  $1/e$  lifetime, pseudodiffusion, and related phenomena, all of which were also observed in the  ${}^3P_0$  state of  $\text{LaF}_3:\text{Pr}^{3+}$ . As mentioned previously, these observations were done in higher concentration samples. In particular, the studies of this section were performed at a concentration of 5 mol%.

Figure 13 shows variation in the  $1/e$  lifetime of the  ${}^3P_0$  state observed when the laser is pumping at different positions within the  $({}^3H_4)_1 \rightarrow {}^3P_0$  absorption curve. These positions are indicated to the lower left-hand side of the figure. These variations are accompanied by an asymmetric non-Gaussian excitation spectrum as shown in Fig. 14. Also evident from Fig. 14 is the fact that the excitation spectrum has a more symmetric (and a more Gaussian-like) shape at longer delays; shown is the particular case of  $t = 50 \mu\text{sec}$ . Finally, Fig. 15 shows an effect that seems to be similar to the phenomenon of spectral diffusion discussed in Sec. IV. This effect, termed "pseudodiffusion,"

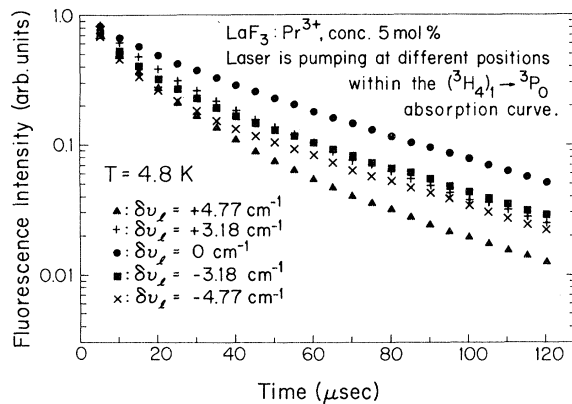


FIG. 13. Variation in the  $1/e$  lifetime of the  ${}^3P_0$  state observed when the laser is pumping at different positions within the  $({}^3H_4)_1 \rightarrow {}^3P_0$  absorption profile. These positions are indicated to the lower left-hand side.  $\delta\nu_l$  is the frequency of the laser with respect to the center of the  $({}^3H_4)_1 \rightarrow {}^3P_0$  absorption profile. The concentration is 5 mol% and the temperature 4.8 K.

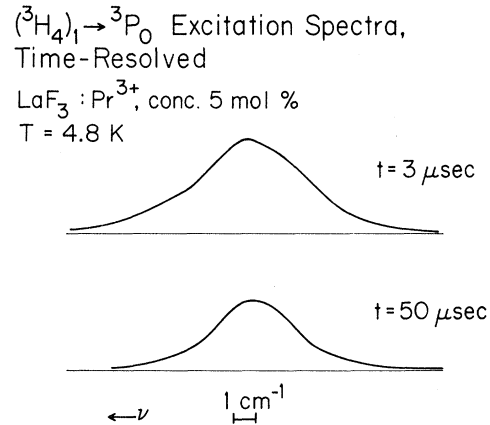


FIG. 14. Time-resolved excitation spectrum depicting the transition  $({}^3H_4)_1 \rightarrow {}^3P_0$ . The concentration is 5 mol% and the temperature 4.8 K.

is observed at  $T = 4.8 \text{ K}$  although simultaneous observations on the resonant transition show that no real spectral diffusion is taking place at this temperature (see Fig. 11). Moreover, this effect is only observed on the edges of the  $({}^3H_4)_1 \rightarrow {}^3P_0$  absorption curve, i.e., in those regions where the greatest shortening of the  $1/e$  lifetime is observed (see Fig. 13).

All of these effects can be accounted for if we assume that they are due to strongly concentration-dependent satellite lines that, at these higher concentrations, are now folded into the broadened main absorption line. In particular, these satellite lines are situated slightly to the high- and low-

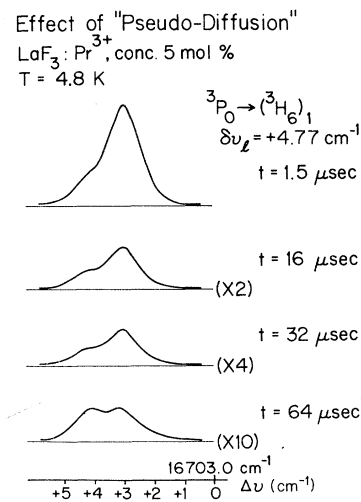


FIG. 15. Effect of "pseudodiffusion" observed for the nonresonant transition  ${}^3P_0 \rightarrow ({}^3H_6)_1$ . The laser is pumping  $4.77 \text{ cm}^{-1}$  to the high-energy side of the center of the  $({}^3H_4)_1 \rightarrow {}^3P_0$  absorption profile. The temperature is 4.8 K and the concentration is 5 mol%.

energy side of the main absorption line, thus accounting for the asymmetric shape of the excitation spectra (Fig. 14), and possess a slightly different nonresonant fluorescence wavelength as well as a shorter  $1/e$  lifetime. The latter two properties account for the variations in lifetime (Fig. 13) and the effect of pseudodiffusion. They also explain why the shape of the excitation spectrum is more symmetric at longer delays (see Fig. 14). Finally the presence of such satellite lines also gives a simple explanation for the line-width and line-shape variations discussed in Sec. III and shown in Fig. 4.

The presence of the type of satellite lines observed in this experiment may also explain deviations from a pure Gaussian line shape which have been observed in classical solid-state spectroscopy.<sup>11</sup> These deviations occur at the wings of the lines, which is the exact behavior expected from the presence of such satellite lines. When doing experiments of lower resolution, the resultant deviations in line shape can then give the erroneous impression of the presence of an additional Lorentzian component.<sup>36,37</sup> Quite generally, we conclude then that, when dealing with linewidth and line-shape measurements in samples of higher concentrations, the possible presence of the type of satellite lines observed in this experiment must be considered and properly accounted for.

Not yet discussed so far is the exact shape of the decay curves shown in Fig. 13. The nonexponential behavior is attributed to crossrelaxation involving the  $^1G_4$  Stark manifold.<sup>38</sup> Attempts to fit these curves to the formula of Inokuti and Hirayama<sup>28</sup> were however unsuccessful. This may be due to the fact that deviations from the above formula that occur at very early delays<sup>31</sup> were not included in these fits. Another possibility is that two or more decay curves of different lifetimes and of different cross-relaxation rates may be superimposed. This may result from the presence of the strong satellite lines that are folded into the main line, as has been discussed above. The resultant curve then does not follow the simple formula of Ref. 28 and a fit will be unsuccessful. Such effects have recently been seen in glasses.<sup>39</sup> Moreover another interesting aspect of the variations displayed in Fig. 13 is to see what happens to these decay curves at higher temperatures. Because of the spectral diffusion effects discussed in Sec. IV, we would expect that the dissimilarities of Fig. 13 are almost entirely eliminated at higher temperatures; i.e., more specifically we would expect that all the decay curves will display the same qualitative behavior after a short initial decay time of a couple of  $\tau_T$ 's, where  $\tau_T = 1/W_T$  (for a

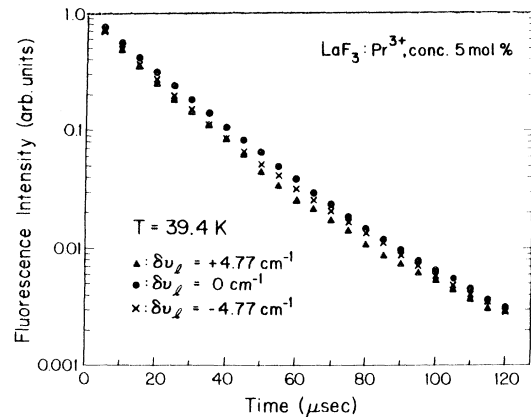


FIG. 16. Repetition of the experiment of Fig. 13, but now the temperature is 39.4 K. Besides the curve corresponding to  $\delta\nu_L = 0$ , the two most divergent curves (i.e., the curves corresponding to  $\delta\nu_L = \pm 4.77 \text{ cm}^{-1}$ ) are indicated.

definition of  $W_T$  see Sec. IV). That this is indeed the case can be seen from Fig. 16. Fig. 16 also shows that the overall decay rate has increased considerably with temperature (compare to Fig. 13). At first glance one might think that this is due to a decrease of the intrinsic lifetime  $\tau_0$ , or to a strong increase in the cross-relaxation rate to the  $^1G_4$  levels. However, the intrinsic lifetime  $\tau_0$  is virtually temperature independent.<sup>38,40</sup> The same is probably also true for the cross-relaxation rate, within the temperature region of interest.<sup>41</sup> The most likely cause for this increase in decay rate is then diffusion to "traps" or "sinks,"<sup>42</sup> very likely traps being, e.g., those ions that give rise to the satellite structure discussed above. These ions have a considerably higher decay rate than all the other ions within the ( $^3H_4$ )<sub>1</sub> →  $^3P_0$  absorption curve, and their function as traps could therefore be quite effective. More generally, our system has probably reached the region of "diffusion-limited relaxation"<sup>42</sup> at these higher temperatures. In principal it should therefore be possible to compare the shape of the decay curves in Fig. 16 with theory,<sup>43</sup> the corresponding diffusion constants<sup>43</sup> being given by way of the transfer rate  $W_T$  which has been determined in Sec. IV. However such a comparison is complicated in our case because, among other things, the main fluorescence is distorted by the presence of the satellite lines, and the trap concentration is not exactly known. We reserve, therefore, such an investigation for a system where the relevant parameters are more clearly known.

## VI. CONCLUSION

The technique of FLN, applied in its time-resolved mode, has proven to be a powerful tool

in investigating the more detailed aspects in the behavior of rare-earth ions doped into a crystalline host. In particular, by extending the investigation to higher-concentration samples, effects such as accidental coincidence, linewidth and line-shape variations, phonon-assisted spectral diffusion, variation of the  $1/e$  lifetime across the absorption profile, pseudodiffusion, etc., have been observed. These are all processes which have previously not been observable directly with classical methods. By extending these investigations to other rare-earth and transition-metal ions, further insight into the behavior of these ions could be obtained. In particular this could clarify, e.g., the exact nature of the phonon-assisted diffusion processes discussed in Sec. IV,

and would possibly allow a direct analytical comparison between the results of these time-resolved studies and the conventional type of investigation involving solely the measurement of decay curves.

#### ACKNOWLEDGMENTS

We would like to thank F. L. Roesler and his group for invaluable help, and for lending us some of the equipment that has made this experiment possible. We are greatly indebted to D. L. Huber for many helpful discussions. We also wish to thank I. S. Shahin for contributing to the initial phases of this work. One of us (W. M. Y.) would also like to acknowledge many fruitful discussions with M. J. Weber and J. A. Paisner.

†Work supported by the NSF under Grant No. DMR-73-02478-A01.

<sup>1</sup>See, for example, T. W. Hänsch, I. S. Shahin, and A. L. Schawlow, *Phys. Rev. Lett.* **27**, 707 (1971); and *Nature (Lond.)* **235**, 63 (1972).

<sup>2</sup>See, for example, F. Biraben, B. Cagnac, and G. Grynberg, *Phys. Rev. Lett.* **32**, 643 (1974); M. D. Levenson and N. Bloembergen, *ibid.* **32**, 645 (1974); T. W. Hänsch, K. C. Harvey, G. Meisel, and A. L. Schawlow, *Opt. Commun.* **11**, 50 (1974).

<sup>3</sup>See, for example, A. Szabo, *Phys. Rev. Lett.* **27**, 323 (1971); **25**, 924 (1970).

<sup>4</sup>This would include having the probe beam frequency variable such that it could be scanned across the absorption profile to measure the width of the "hole" burned by the saturation beam. Another possibility, in case of cw-laser spectroscopy, is to simply amplitude modulate the saturation beam, see A. Szabo, *Phys. Rev. B* **11**, 4512 (1975).

<sup>5</sup>This is due to the low oscillator strength of the transitions involved. The great majority of the commonly observed optical transitions in solids are parity forbidden, leading to small oscillator strengths of typically only about  $10^{-6}$ . An approximate way on how to take into account transient effects that occur when the length of the laser pulse is comparable to or shorter than the lifetime of the excited state is given in I. S. Shahin, Ph.D. thesis (Stanford University, 1972), M. L. Report No. 2099 (unpublished); I. S. Shahin and T. W. Hänsch, *Opt. Commun.* **8**, 312 (1973).

<sup>6</sup>Not mentioned so far has been the fact that FLN is limited to metastable levels, i.e., to those levels that have a finite quantum yield. This is no great restriction since most other levels are homogeneously broadened due to a high nonradiative decay rate.

<sup>7</sup>R. Flach, D. S. Hamilton, P. M. Selzer, and W. M. Yen, *Phys. Rev. Lett.* **35**, 1034 (1975).

<sup>8</sup>R. Flach, D. S. Hamilton, P. M. Selzer, and W. M. Yen, *Bull. Am. Phys. Soc.* **20**, 446 (1975).

<sup>9</sup>P. M. Selzer, D. S. Hamilton, R. Flach, and W. M. Yen, *J. Lumin.* **12/13**, 737 (1976).

<sup>10</sup>R. Flach, I. S. Shahin, and W. M. Yen, *Appl. Opt.* **13**, 2095 (1974).

<sup>11</sup>W. M. Yen, W. C. Scott, and A. L. Schawlow, *Phys. Rev.* **136**, A271 (1964).

<sup>12</sup>R. Solomon and L. Mueller, *Appl. Phys. Lett.* **3**, 135 (1963).

<sup>13</sup>N. Takeuchi and A. Szabo, *Phys. Lett. A* **50**, 361 (1974).

<sup>14</sup>A. Szabo and N. Takeuchi, *Opt. Commun.* **15**, 250 (1975).

<sup>15</sup>The data for the 0.2-mol% sample was taken with the laser pumping in the center of the  $(^3H_4)_1 \rightarrow ^3P_0$  absorption profile. The data for the 5-mol% sample was recorded with the laser pumping  $4.77 \text{ cm}^{-1}$  to the low-energy side, which was necessary to avoid masking of the narrowed fluorescence by the inhomogeneous background. This background appears at higher temperatures due to the spectral diffusion effect discussed in Sec. IV and Ref. 7. Due to the strong increase of this background with temperature no reliable data could be taken for the 5-mol% sample above a temperature of 26 K. It was assumed that possible variations in the homogeneous width across the absorption profile, resulting from changes in the ion-lattice coupling constants, are negligible.

<sup>16</sup>W. B. Gantrud and H. W. Moos, *J. Chem. Phys.* **49**, 2170 (1968).

<sup>17</sup>L. A. Riseberg and H. W. Moos, *Phys. Rev. Lett.* **19**, 1423 (1967).

<sup>18</sup>L. E. Erickson, *Opt. Commun.* **15**, 246 (1975).

<sup>19</sup>This splitting is expected to disappear to first order, see A. Abragam and B. Bleaney, *Electron Paramagnetic Resonance of Transition Ions* (Clarendon, Oxford, 1970). Using a cw-dye laser, Erickson (see Ref. 18) obtained an upper limit of 10 MHz for the size of this splitting in the  $(^1D_2)_1 \rightarrow (^3H_4)_1$  resonant transition. It is reasonable to assume that the upper limit for the  $^3P_0 \rightarrow (^3H_4)_1$  and  $^3P_0 \rightarrow (^3H_6)_1$  transitions is of the same order of magnitude or even smaller.

<sup>20</sup>N. Motegi and S. Shionoya, *J. Lumin.* **8**, 1 (1973).

<sup>21</sup>A. Zalkin, D. H. Templeton, and J. E. Hopkins, *Inorg. Chem.* **5**, 1946 (1966).

<sup>22</sup>This same effect has recently also been observed in glasses, see T. Kushida and E. Takushi, *Phys. Rev. B* **12**, 824 (1975). See also Ref. 39.

<sup>23</sup>See also, e.g., Ref. 3, or L. A. Riseberg, *Phys. Rev. A* **7**, 671 (1973).

- <sup>24</sup>The reason for this is that  $\Delta\nu_a$  does not vary much across the  $(^3H_4)_1 \rightarrow ^3P_0$  absorption profile (see also Fig. 5). This has already been an implicit assumption when  $\Delta\nu'_e$  was written in the simple form of Eq. (2).
- <sup>25</sup>Following Ref. 11 the contribution of the Raman term is less than 5% of the total linewidth for both, the resonant and nonresonant transition, up to a temperature of 40 K. The  $^3P_0$  state contributes to the linewidth only via the Raman process. The neglect of the Raman term amounts then to the disregard of any linewidth contributions from the  $^3P_0$  state.
- <sup>26</sup>D. L. Dexter, *J. Chem. Phys.* **21**, 836 (1953).
- <sup>27</sup>R. Orbach, in *Optical Properties of Ions in Crystals*, edited by H. M. Crosswhite and H. W. Moos (Interscience, New York, 1967), p. 445.
- <sup>28</sup>M. Inokuti and F. Hirayama, *J. Chem. Phys.* **43**, 1978 (1965). [The same formula, with  $s=6$ , was originally derived by Th. Förster, *Z. Naturforsch. A* **4**, 321 (1949).]
- <sup>29</sup>This might have been possible for the 20-mol% sample, where all the data were taken on the nonresonant transition. Since in this case the value of  $\Delta\nu_a$  (see Sec. III) was close to half the value of  $\Delta\nu_{inh}$ , the recorded fluorescence profiles were not very sensitive to possible variations of  $K(\Delta E, T)$  as a function of  $\Delta E$ .
- <sup>30</sup>To our knowledge, there is no theoretical treatment that has expanded the calculations of Inokuti and Hirayama (see Ref. 28) to include the case where  $K(\Delta E, T)$  depends on  $\Delta E$ . Our assumption is based on the fact that, within the experimental accuracy,  $H(t)$  followed the above formula in all of our data.
- <sup>31</sup>See, e.g., R. K. Watts, in *Optical Properties of Ions in Solids*, edited by B. Di Bartolo (Plenum, New York, 1975), p. 323.
- <sup>32</sup>The fit of our data to the formula of Ref. 28 was quite insensitive to the value of  $s$ . The analysis was carried out with  $s=6$ , based on the fact that the transition involved is quadrupole forbidden. This value has been confirmed in Ref. 9. However, in a more extensive analysis deviations from Eq. (7) have to be considered, see, e.g., W. P. Wolf and R. J. Birgeneau, *Phys. Rev.* **166**, 376 (1968); and T. Holstein, S. K. Lyo, and R. Orbach, *Phys. Rev. Lett.* **36**, 891 (1976). This makes a slightly different, heuristic value of  $s$  possible.  $W_T$  is then not expected to scale exactly as  $C^2$ , as implied by Eq. (8).
- <sup>33</sup>R. Orbach and M. Tachiki, *Phys. Rev.* **158**, 524 (1967).
- <sup>34</sup>Wm. S. Heaps, L. R. Elias and W. M. Yen, *Phys. Rev. B* **13**, 94 (1976).
- <sup>35</sup>W. T. Carnall, P. R. Fields, and R. Sarup, *J. Chem. Phys.* **51**, 2587 (1969). A two-photon process would also have shown a strong nonlinear dependence on the laser intensity (as well as the energy density), and it would have been concentration independent, whereas no spectral diffusion could be observed in our experiment for low-concentration samples.
- <sup>36</sup>W. M. Yen, R. L. Greene, W. C. Scott, and D. L. Huber, *Phys. Rev.* **140**, A 1188 (1965).
- <sup>37</sup>D. S. Hamilton, P. M. Selzer, D. L. Huber, and W. M. Yen, *Phys. Rev. B* **14**, 2183 (1976).
- <sup>38</sup>M. R. Brown, J. S. S. Whiting, and W. A. Shand, *J. Chem. Phys.* **43**, 1 (1965).
- <sup>39</sup>M. J. Weber, J. A. Paisner, S. S. Sussman, W. M. Yen, L. A. Riseberg, and C. Brecher, *J. Lumin.* **12/13**, 729 (1976).
- <sup>40</sup>M. J. Weber, *J. Chem. Phys.* **48**, 4774 (1968).
- <sup>41</sup>This process involves either the emission of phonons to dispose of an energy surplus of  $268\text{ cm}^{-1}$ , or otherwise it involves the absorption of a phonon, providing for an energy deficit of  $77\text{ cm}^{-1}$ .
- <sup>42</sup>See, e.g., M. J. Weber, *Phys. Rev. B* **4**, 2932 (1971); J. P. van der Ziel, L. Kopf, and L. G. Van Uitert, *ibid.* **B 6**, 615 (1972).
- <sup>43</sup>See, e.g., P. G. de Gennes, *J. Phys. Chem. Solids* **7**, 345 (1958); M. Yokota and O. Tanimoto, *J. Phys. Soc. Jpn.* **22**, 779 (1967); R. K. Watts, in Ref. 31. See also Ref. 42.